processes

MDPI

Article

Aluminium-Assisted Alloying of Carbon Steel in Submerged Arc Welding with Al-Cr-Ni Unconstrained Metal Powders: Thermodynamic Interpretation of Gas Reactions

Theresa Coetsee * and Frederik De Bruin

Department of Materials Science and Metallurgical Engineering, University of Pretoria, Pretoria 0002, South Africa
* Correspondence: theresa.coetsee@up.ac.za

Abstract: Unconstrained metal powders of chromium and nickel, in combination with aluminium, were used in the submerged arc welding (SAW) process to simplify weld metal alloying. Unconstrained metal powders refer to non-alloyed metal powders that are not constrained in tubular wire, such as fluxed-cored and metal-cored wire. Aluminium powder is used to control the oxygen potential at the molten flux–weld pool interface. The results presented here show that the addition of aluminium powder to the weld metal enhances Cr and Ni yields to 89% for Cr and 91% for Ni, compared to lower values reported in pre-alloyed powder application. Alloying of the carbon steel in the base plate and weld wire combination was achieved at 6.0% Cr, 6.2% Ni, and 4.5% Al, with the weld metal oxygen controlled to 162 ppm O. Thermodynamic analysis was applied to investigate the likely gas reactions in the arc cavity emanating from the chemical interaction between Cr, Ni, and Al. The effects of gas-based chemical reactions on the yield of Cr and Ni to the weld pool are discussed and incorporated into our SAW reaction flow diagram. Overall SAW process productivity gains can be accomplished by using unconstrained metal powders to alloy the weld metal because expensive and time consuming steps, such as the manufacturing of alloyed wire and alloyed powder, can now be eliminated.

Keywords: pyrometallurgy; powder; nickel; chromium; oxygen control; aluminium; welding

Citation: Coetsee, T.; De Bruin, F. Aluminium-Assisted Alloying of Carbon Steel in Submerged Arc Welding with Al-Cr-Ni Unconstrained Metal Powders: Thermodynamic Interpretation of Gas Reactions. *Processes* **2022**, *10*, 2265. https://doi.org/10.3390/pr10112265

Academic Editor: Mingxia Gao

Received: 25 August 2022
Accepted: 29 October 2022
Published: 2 November 2022

1. Introduction

Submerged arc welding (SAW) is used as a high-productivity welding method in heavy engineering industries to join thick steel plates, for example in the building of large seafaring ships [1]. In addition to arc formation between the weld wire tip and the base plate material, and the consequent melting of the weld wire, complex physical and chemical interactions of heat and mass transfer occur in the arc cavity [1]. Chemical reactions between the molten steel weld pool and its covering slag (molten flux) continue until the weld pool is solidified as weld metal [2,3].

The weld metal composition is influenced by applied welding parameters of voltage, current, polarity, and welding speed, and by slag-steel-gas chemical reactions in the weld pool and arc cavity [3–5]. The weld pool reaction time is set by heat input, which is in turn set by the combination of voltage, current and welding speed [6]. Although these welding parameters are highly important parameters in the SAW process, the weld metal chemistry is mostly set by the flux composition, which in turn sets the oxygen potential in the arc cavity [4,7]. Flux compositions are designed to achieve specific weld metal chemistries through element transfer between the slag and the weld pool [3,8–11]. Slags must also exhibit specific physico-chemical properties to facilitate the SAW process. For example, the flux composition is formulated to ensure optimum levels of slag surface tension and slag viscosity to sufficiently shield the weld pool from atmospheric gasses by covering the weld bead completely. The flux is also formulated to ensure that the slag liquidus temperature

is 50 °C lower than the weld metal solidification temperature to ensure sufficient reaction time between the weld pool and slag for chemical reactions and inclusion removal [4–6,8].

SAW fluxes are formulated from a combination of oxides and fluorides. The fluoride compound in the flux is typically CaF_2. Through experimental measurements, it has been concluded that the flux composition basicity index (BI), as displayed in Equation (1), should be larger than 1.5. This requirement is set to limit the weld metal hydrogen content and to ensure that the weld metal total oxygen content (ppm O) is at 250 ppm O [12,13]. The latter value stems from the empirical data trend showing constant total weld metal oxygen content of 250 ppm at BI values higher than 1.5 [13].

$$\mathrm{BI} = \frac{\%CaF_2 + \%CaO + \%MgO + \%BaO + \%SrO + \%Na_2O + \%K_2O + \%Li_2O + 0.5(\%MnO + \%FeO)}{\%SiO_2 + 0.5(\%Al_2O_3 + \%TiO_2 + \%ZrO_2)} \quad (1)$$

Total ppm O in the weld metal is a critical weld metal materials property control variable because oxide inclusions are formed from this oxygen. If too many inclusions are formed in the weld metal the effect is weakened materials properties, specifically the weld metal impact toughness is decreased. On the other hand, oxide inclusions are required in the weld metal to form nucleation sites to induce acicular ferrite (AF) microstructure formation. An AF microstructure is associated with improved materials properties, such as tensile stress and impact toughness. The acceptable total ppm O level in carbon steel was identified as 200 ppm O to 500 ppm O because sufficiently high weld metal impact toughness values were measured at these weld metal total oxygen content values [14]. Similarly, the weld metal total ppm O in chromium containing steels must also be controlled to improve weld metal impact toughness [15]. Much higher ppm O values were analysed in the metal droplets formed from the molten weld wire that are subsequently transferred into the weld pool, as much as 2000 to 3000 ppm O [16,17]. Therefore, as highlighted above, this initially high oxygen content in the weld pool must be decreased to the lower levels of 200 ppm O to 500 ppm O in the weld metal to ensure sound materials properties of the weld metal.

It has been proven that the decomposition of molten flux (slag) oxides in the high-temperature environment of the arc plasma is the reason for oxygen added to the weld metal [18]. The arc plasma stability order of oxides in the flux was measured from welding tests with binary mixtures of CaF_2-oxide fluxes under Argon. The total ppm O analysed in the weld metal following the welding test, indicates the arc plasma stability of the oxide in the CaF_2-oxide flux, with a less stable oxide resulting in higher weld metal total ppm O. The authors found the stability order of the oxides from most stable to least stable to be as follows: CaO, K_2O, Na_2O and TiO_2, Al_2O_3, MgO, SiO_2, and MnO [18]. Increased flux CaF_2 content is applied to dilute the proportion of low stability oxides in the flux. The result is decreased weld metal ppm O because less oxygen is introduced into the arc cavity via the lesser quantity of low stability oxides in the flux. Weld metal is usually alloyed with nickel from the weld wire because it has a relatively low affinity for oxygen and therefore is not expected to oxidise significantly in the arc cavity. Even though chromium does have a high affinity for oxygen, chromium and nickel are often alloyed via weld wire made of a particular stainless steel grade. The consequence is that the weld wire chemistry is usually over matched to the base plate composition. Since weld wire is used as the alloying source for chromium and/or nickel, the fluxes applied in SAW of chromium and/or nickel containing steel contain little to zero metals and oxides of chromium and/or nickel, resulting in neutral or non-alloyed flux formulations [19]. Chromium, nickel, molybdenum, or niobium metal powders may be added to the flux to compensate for element loss across the arc [20]. Manufacturing of weld wires of specific compositions is expensive and time consuming. Consequently, only a number of weld wire formulations are available, and these weld wires cannot closely match all desired alloy compositions.

It is claimed that better alloy matching of the weld metal to the base plate material may be accomplished if metal powder is applied to the welding process instead of using weld wire only [21]. Chromium-nickel pre-alloyed iron based powders were applied in coating applications using SAW to better control the chemistry specification of the

applied coating [21]. The main claimed benefit of using pre-alloyed powders for alloying in cladding, compared to alloying via the weld wire, is that alloying element dilution of the weld metal from the iron contained in the weld wire and the substrate steel is limited. Dilution from the weld wire is limited because higher alloy concentrations can be accommodated in the pre-alloyed powder, compared to that in the weld wire. Dilution from the substrate steel iron is limited because less of the substrate steel is melted into the weld pool due to the weld pool being effectively cooled as some of the arc heat is used to melt the added powders, instead of melting the substrate steel. The overall deposition productivity is also improved due to the application of metal powders. From the reported application examples of pre-alloyed powders in SAW the Ni and Cr yield values were as follows: nickel yield values ranged from 57% to 78% and chromium yields varied from 56% to 76%. The pre-alloyed iron based powders contained 27–29% Cr, 5–8% Ni, and 2–4% Mo [21]. The Ni and Cr yield values varied in tandem, with both the Ni and Cr yield values at a lower level or a higher level in each SAW application test. Lower Ni and Cr yields seem to be associated with lower powder feed rates. These yield values are significantly lower compared to the typical literature reported yields from SAW with solid weld wire, namely zero nickel loss and only a slight loss of chromium were reported [19,22].

Few cases of higher nickel and chromium loss values were reported from alloying via solid weld wire in SAW [23]. One study confirmed the effect of slag chemistry on nickel and chromium loss from the weld pool. The nickel and chromium content of the base plate steel and weld wire were low: the base plate steel contained 1.65% Ni and 0.76% Cr and the solid weld wire contained 0% Ni and 1.25% Cr. The maximum loss of nickel and chromium, relative to the nominal compositions, were reported as 0.3% each. Although 0.3% is a small quantity, relative to the 1.65% Ni and 0.76% Cr in the base plate steel, these values translate to 82% Ni yield and 61% Cr yield in the presence of a highly oxidising flux of 40% SiO_2-MnO-CaO [23]. In the same study, in welding tests with a more oxidising flux containing FeO the element loss values for Ni and Cr were lower than the numbers mentioned above, and welding with a highly reducing basic flux of 40% SiO_2-MnO-CaF_2 showed the lowest element loss values for Ni and Cr [23]. Therefore, it seems that the chemical interaction between chromium and nickel, and the chemical interaction between these alloying elements and the flux are not widely studied or reported.

Aluminium is typically not added in large quantities into steel as it is only added as de-oxidiser element in the steelmaking process. For example, de-oxidation of 16% Cr steel with aluminium to 1% Al at 1650 °C resulted in the equilibrium total oxygen content of the steel at 30 ppm O [24]. This level of total ppm O is much lower than the typically measured values of total ppm O measured in SAW weld metal. Therefore, the application of aluminium in SAW must be carefully considered so as to maintain sufficient total ppm O in the weld metal for inclusion formation.

More recently aluminium has been applied in the development of low density steels for the automotive industry [25]. Similarly, aluminium is used in the development of low density stainless steels [26]. In the same way as applied in high-entropy alloys, aluminium is used in high-entropy steels to induce high configurational entropy in the steel matrix. In this new class of steels the play-off between high tensile stress and high ductility prevailing in older steel formulations is removed as the high-entropy steel chemistry formulation can now provide excellent properties overall [27]. Therefore, the application of combinations of alloying elements with aluminium in SAW is an important contribution to expanding the application of SAW to these newer steel grades.

Few studies were published on the application of unconstrained metal powders, meaning not fluxed cored wire or metal cored wire, as alloying method in SAW. The chemical behaviour of nickel and chromium when applied in SAW as an alloying powder is not clear because the yield of nickel and chromium from the alloying powders to the weld metal appears to be much lower than 100% yield [19,22]. The latter number of 100% is typically reported for nickel and chromium yields in SAW when weld wire is used as alloy carrier [19,22]. The objective of this study is firstly, to demonstrate the application

of unconstrained nickel, chromium, and aluminium powders in SAW to alloy the weld metal and control the weld metal oxygen content. The secondary objective is to apply thermodynamic analyses to elucidate the chemical interaction between Ni, Cr, and Al in SAW and its influence on Ni yield and Cr yield from unconstrained metal powders to the weld pool. Overall SAW process productivity gains can be made by using unconstrained metal powders to alloy the weld metal because expensive and time consuming steps, such as the manufacturing of alloyed wire and/or alloyed powder, can now be eliminated [21].

2. Materials and Methods

2.1. Welding Tests

One SAW test run was made without the addition of metal powders in order to generate a base case (BC) weld for comparison to welds made with metal powder additions. After the base case was established for a set of weld parameters, the same parameters were applied in the MP8 weld in which metal powders were also added. The metal powders consisted of pure powders, namely chromium, nickel, and aluminium in equal mass proportions of 7 g each. The bead-on-plate weld run length was typically 260 mm in length on a 350 mm length steel plate. The plate thickness was 12 mm and the plate width was 300 mm. Welding parameters were 500 A and 28 V at a 42 cm/minute travel speed to provide a heat input value of 2.0 kJ/mm. DCEP (direct current electrode positive) welding was performed.

2.2. Materials and Analyses

Structural steel of grade S355J2+N was used as base plate material since it is a widely available steel formulation in South Africa. Weld wire with a 3.2 mm diameter was sourced from Afrox Ltd., Johannesburg, South Africa. Optical emission spectroscopy (OES) was used to analyse the base plate steel major element content values. The combustion method was used to analyse total oxygen content in the base plate and weld wire. The complete analysis of the base plate steel is shown in Table 1. The weld wire composition for the remaining elements, as displayed in Table 1, are from the supplier's analysis sheet.

Removal of the weld metal sample for chemical analysis required the following procedure. Weld bead cross-section cuts were made at the middle position of the weld run by using a band saw. Subsequently, a manual saw was used to cut individual volume samples of the weld metal from each cross-section. In order to only cut the weld metal from the cross-section cut, the cross-section interface was first prepared by levelling and etching with 2% Nital solution. Three volume samples from the cross-section cuts were analysed by using different analysis methods. One sample was analysed by inductively coupled plasma optical emission spectroscopy (ICP-OES) to determine the major element composition of the sample. The second sample was analysed by combustion method for carbon and total oxygen content. The third weld metal sample was analysed by SEM (scanning electron microscope) to confirm the bulk chemical analysis of the weld metal. The polished section was prepared for SEM analysis by polishing the sample to a mirror finish, followed by etching with 2% Nital solution to reveal the weld metal boundary in the base plate. The SEM work was completed with a Zeiss (Oberkochen, Germany) crossbeam 540 FEG (Field emission gun) SEM with EDS (energy dispersive spectrometer), operated at 20 kV.

An agglomerated commercial flux (0.2–1.6 mm agglomerate particle size) was used in the SAW test runs. The flux is an aluminate basic flux with flux basicity, as displayed in Equation (1), at 1.4. The flux bulk chemical composition is shown in Table 2 for reference, even though the flux chemistry and mineralogy were previously extensively investigated [28]. An important consideration in the selection of a flux for this work is the thermodynamic stability of the flux in the presence of aluminium metal. Therefore, the aluminate basic flux was selected following initial testing of different fluxes [28]. Metal powders of pure Al (99.7% Al) supplied by Sigma-Aldrich, pure Ni (99.5% Ni) supplied by GoodFellow, and pure Cr (99.0% Cr) supplied by Alfa Aesar were used.

Table 1. Carbon steel base plate and weld wire compositions (mass%) [29].

	%C	%Si	%Mn	%O	%Al	%P	%S	%Ti	%Cu	%Cr	Balance
Plate	0.120	0.155	1.340	0.0007	0.067	0.019	0.007	0.005	0.030	0.160	Fe
Wire	0.110	0.137	0.990	0.0003	0.000	0.009	0.023	0.000	0.140	0.000	Fe

Table 2. Flux bulk chemical composition (mass%) [28].

MnO	CaO	SiO_2	Al_2O_3	CaF_2	MgO	FeO	TiO_2	Na_2O	K_2O
6.8	0.1	19.6	24.9	17.9	22.2	2.4	1.0	1.6	0.2

2.3. Thermochemical Calculations

A thermodynamic analysis of gas phase reactions was performed in FactSage 7.3 thermochemical software [30]. As a first approximation, simple gas phase reactions were considered to quantify the possible reaction paths of metal fluoride formation in the arc cavity due to reactions involving metal vapour, fluorides, and oxides in the slag. The Gibbs free energy values were calculated in the Reaction module of FactSage 7.3 thermochemical software. The temperature interval of 1600 °C to 2500 °C was used in these calculations because this is the temperature band of the main reactions in SAW as identified in previous works, ranging from close to the liquidus temperature of steel (1600 °C) to the maximum temperature reported for the arc plasma–weld pool interface (2500 °C) [2–4]. The effective slag-metal equilibrium reaction temperature in SAW is accepted as 2000 °C, and is then also included in this temperature interval applied in the calculations displayed in Section 4.1. A more complex approximation of a likely gas phase species formation was made in the Equilib module in FactSage 7.3 thermochemical software by calculating the equilibrium of gas, slag, and metal powder inputs as equilibrium phases of gas, molten flux (slag), and molten alloy. This gas-slag-metal equilibrium model is similar to the simulation model that was previously successfully applied to calculate the carbon steel weld metal total ppm O for different flux formulations in SAW [29]. The proportion of the feed aluminium quantity that possibly participated in the gas reactions was varied to gauge the role of aluminium in the gas phase reactions. The thermodynamically predicted gas phase species from these calculations were used to interpret the likely gas phase reaction changes due to chromium, nickel, and aluminium added to the SAW process. The FToxid, FSstel, and FactPS databases were selected and the selection was made for the inclusion of plasma species [30]. The results are reported in Section 4.1.

3. Results

3.1. Chemical Analyses

The weld metal compositions from each of the SAW test runs are shown in Table 3, namely the reference test run without metal powder addition (BC) and the test run with metal powder addition (MP8). Figure 1 displays the SEM micrograph with marked areas of the EDS analyses shown in Table 4. The EDS analyses in Table 4 confirm alloying of the weld metal with the added metal powders of nickel, chromium, and aluminium. The area shown in Figure 1 and used for EDS analyses is positioned at the geometric centre of the weld metal cross-section.

Table 3. Bulk chemical composition of weld metals (mass%) [29].

	%C	%Si	%Mn	%O	%Al	%P	%S	%Ni	%Cr	%Fe
Base Case	0.110	0.260	1.300	0.0499	0.032	0.022	0.011	0.005	0.110	98.03
MP8	0.098	0.560	1.637	0.0162	4.483	0.021	0.008	6.213	6.017	80.77

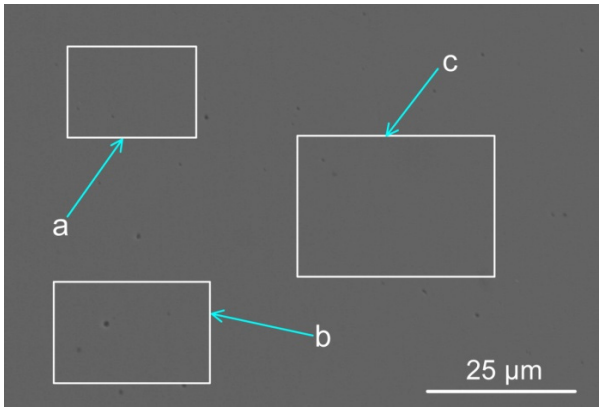

Figure 1. Scanning electron microscope micrograph of weld metal areas marked a, b, and c (see Table 4 below, indicating the analyses per marked phase area: a, b, and c) (×3000).

Table 4. SEM-EDS analyses of areas a, b, and c in Figure 1 (mass%).

	%Si	%Mn	%Al	%Ni	%Cr	%Fe
a	1.10	1.90	5.20	6.70	6.60	78.5
b	1.10	1.80	5.30	6.60	6.60	78.6
c	1.10	1.80	5.39	6.39	6.59	78.7

The slight increase in the silicon and manganese content of the MP8 weld metal, as compared to the BC weld metal, is due to the aluminothermic reduction in MnO and SiO_2 content from the slag. This effect was identified in our previously reported work on aluminium-assisted alloying of different metal powders in SAW [31–37]. The total ppm O in the MP8 weld metal was significantly lowered (162 ppm O) as compared to the BC weld metal (499 ppm O). This lowering to 162 ppm O in the MP8 weld metal is due to the de-oxidiser effect of aluminium at the weld pool–slag interface [31–37].

3.2. Mass Balance

A mass balance was conducted to quantify the yield of nickel, chromium, and aluminium from the metal powders to the weld metal. Mass measurements and mass balance calculations were combined as described in this section. This calculation procedure is the same procedure applied in our previous studies [33–37]. The steel plate mass was measured before and after the SAW test run. This mass difference was used to quantify the mass of weld wire and metal powder added to the weld metal run. The stereoscope image (Figure 2) of the etched weld metal cross-section was used to measure the weld metal areas above and below the base plate top surface level. These areas are marked in Figure 2 for both weld metal cross-section images and are named as follows. Area 1 equals the area between line A and line B and is the proportional area above the base plate top surface level. This is the proportion of the weld metal that was contributed from the weld wire and metal powder melted into the weld pool, namely Area 1. Area 2 equals the area between line B and line C and is the proportion of the weld metal area that was contributed from the melting of the base plate. Here, this area ratio is defined as the dilution ratio as previously reported and named ($\%DR_{(wire+MP)}$) in the following expressions [33–37].

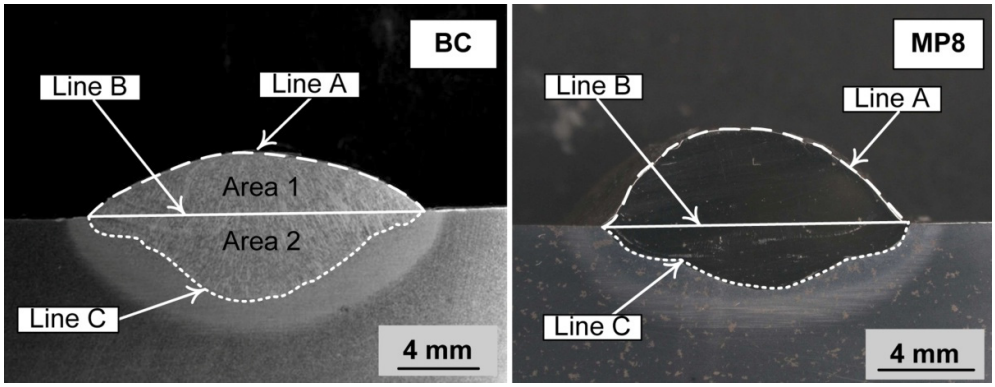

Figure 2. Stereoscope micrographs of the weld metal cross-sections.

The mass of aluminium, chromium, and nickel added to the SAW test run were calculated from Equations (2)–(4). The weld metal composition in Table 3 was used as input to Equation (4). As an example, the expressions in Equations (2)–(4) illustrate the calculation sequence for aluminium. In the same way, the calculations for chromium and nickel were made by using the %Cr or %Ni in the weld metal, shown in Table 3, as the input for Equation (4).

$$\%DR_{(wire+MP)} = \left(\frac{A_{(wire+MP)}}{A_{(wire+MP)} + A_{BP}}\right) \times 100 = \left(\frac{Area1}{Area1 + Area2}\right) \times 100 \quad (2)$$

$$m_{WM} = (m_{wire} + m_{MP}) \times \left(\frac{100}{\%DR_{(wire+MP)}}\right) \quad (3)$$

$$(\text{gram Al to WM}) = (m_{WM}) \times \left(\frac{\%Al_{WM}}{100}\right) \quad (4)$$

where WM = weld metal; MP = metal powder; BP = base plate; wire = weld wire; m = mass (gram); A = area (mm^2).

Once the grams of nickel, chromium, and aluminium added to the weld metal test run were calculated from Equations (2)–(4), the percentage yield of each element from the metal powder to the weld metal was calculated from the initial input masses of 7 g of Ni, 7 g of Cr, and 7 g of Al. The numbers applied in Equations (2)–(4) and the calculation results from Equation (4) are displayed in Table 5. The resultant percentage yield numbers for Ni, Cr, and Al are 91%, 89%, and 67%, respectively.

Table 5. Mass balance numbers and percentage yield calculation results for Al, Ni, and Cr.

	Al (g)	**Ni (g)**	**Cr (g)**	**Powder (g)**	**Wire (g)**	**Base Plate (g)**	**Weld Metal (g)**	**%DR$_{(wire+MP)}$**	**%Al Yield**	**%Ni Yield**	**%Cr Yield**
Base Case	0	0	0	0	33.8	33.8	67.6	50	0	0	0
MP8	4.7	6.5	6.3	17.5	52.5	34.5	104.5	67	67	91	89

3.3. Exothermic Reactions Quantified

Aluminothermic reduction reactions in Equations (5) and (6) definitely occurred. This is confirmed by comparison of the MP8 and BC weld metal analyses in Table 3. It can be seen that the silicon and manganese content in the MP8 weld metal increased compared to the silicon and manganese content of the BC weld metal formed without any metal powder additions. In addition, the aluminothermic reduction reactions in Equations (7) and (8) are also considered possible, although the extent of these reactions is less clear than that of the reactions in Equations (5) and (6). It was confirmed from our previous similar works on SAW, with

different metal powder combinations with aluminium powder added as the de-oxidiser, that FeO formed in the slag from the excess oxygen transferred from the arc cavity [31–37]. This FeO may also be reduced by aluminium powder via reaction (7) to control the oxygen potential at the weld pool–slag interface [31–37]. As discussed previously, chromium oxide can be reduced by aluminium via Equation (8) [33].

$$3(SiO_2) + 4(Al) = 3(Si) + 2(Al_2O_3) \quad \Delta H^{\circ}_{2000^{\circ}C} = -82.1 \text{ kJ/mol Al} \tag{5}$$

$$3(MnO) + 2(Al) = 3(Mn) + (Al_2O_3) \quad \Delta H^{\circ}_{2000^{\circ}C} = -248.4 \text{ kJ/mol Al} \tag{6}$$

$$3(FeO) + 2(Al) = 3(Fe) + (Al_2O_3) \quad \Delta H^{\circ}_{2000^{\circ}C} = -416.5 \text{ kJ/mol Al} \tag{7}$$

$$3(CrO) + 2(Al) = 3(Cr) + (Al_2O_3) \quad \Delta H^{\circ}_{2000^{\circ}C} = -326.6 \text{ kJ/mol Al} \tag{8}$$

( ): liquid.

The pick-up of silicon and manganese in the MP8 weld metal relative to the base case (BC) weld metal analysis is confirmation that sufficient contact time was established between the aluminium powder and the flux to enable reactions (5) and (6) to proceed to a significant extent. The Al_2O_3 formed as the product in reactions (5) and (6) was easily absorbed into the molten flux because these reactions occurred at the molten flux–weld pool interface [31–38]. In order to calculate the exothermic reaction heat contributions from Equations (5) and (6), the mass of manganese and silicon added to the weld metal via these reactions must first be quantified by using Equation (9). This calculation procedure was previously reported [33–37]. For example, the mass of Mn added from the aluminothermic reduction (M_{Mn}) is calculated according to Equation (9). The inputs to Equation (9) are the weld metal mass (Mwm) and the dilution ratio value ($\%DR_{(wire+MP)}$), shown in Table 5 for the base case, and the %Mn in the weld metal, shown in Table 3. The square bracketed terms in Equation (9) represent the calculation of the BC weld metal nominal composition.

$$M_{Mn} = (M_{WM})\left(\frac{\%Mn_{WM}}{100} - \left[\frac{\%DR_{wire}}{100} \times \frac{\%Mn_{wire}}{100}\right] - \left[\left(1 - \frac{\%DR_{wire}}{100}\right) \times \frac{\%Mn_{BP}}{100}\right]\right) \tag{9}$$

where M = mass (gram); M_{WM} = mass Mn (gram); $\%Mn_{WM}$ = %Mn in weld metal; $\%DR_{wire}$ = % of weld metal contributed by weld wire in the base case (BC); $\%Mn_{wire}$ = %Mn in weld wire; $\%Mn_{BP}$ = %Mn in base plate (BP); WM = weld metal; BP = base plate; wire = weld wire.

The exothermic heat from reactions (5) and (6) were calculated by using the reaction enthalpy values as displayed next to reactions (5) and (6) in the text above. A simplified translation of the kJ values is made by using the heat capacity of steel (0.460 kJ/kg K) to calculate the expected increase in weld metal temperature due to reactions (5) and (6). From the numbers shown in Table 6, it can be seen that small gram quantities of SiO_2 and MnO were reduced into the weld metal via reactions (5) and (6). However, the amount of exothermic heat released from these reactions is sufficiently large enough to significantly increase the weld metal temperature by 66 °C as displayed in the last column of Table 6. Because this heating effect is instantaneous, the heating effect is significant in the welding process. The exothermic heat may contribute to the melting of metal powders to facilitate its incorporation into the weld pool.

Table 6. Exothermic heat added to the weld pool from reactions (5) and (6).

	SiO_2 (g)	MnO (g)	Al (g)	Reaction (5) (kJ)	Reaction (6) (kJ)	Reactions (5) & (6) (kJ)	Weld Metal ΔT (°C)
MP8	0.93	0.63	0.72	−1.70	−1.48	−3.18	66

Also of importance is considering the weld pool solidification time because it is an important aspect of oxygen content control in the weld pool. The effect is well-described in the literature, as follows: An increased weld pool cooling time ensures an increased period of time for the oxide inclusions to float from the weld pool to the molten slag–weld

pool interface, where it can be absorbed into the molten slag [6]. For the same welding parameters, the weld pool cooling time is set by the difference between the weld pool liquidus and solidus temperatures. Therefore, the weld pool cooling time may be different for different weld pool chemistries. Figure 3 shows the cooling curves for the BC and MP8 weld metal chemistries displayed in Table 3. The solidification curves in Figure 3 were calculated in FactSage 7.3 thermochemical software by using the Equilib module with the FToxid and FSstel databases selected [30]. The calculation results in Figure 3 confirm that the solidus temperature of MP8 weld metal is approximately 100 °C lower than that of the base case (BC) weld metal. This difference at least in part contributes to a lower ppm O in the MP8 weld metal as compared to the BC weld metal, as displayed in Table 3.

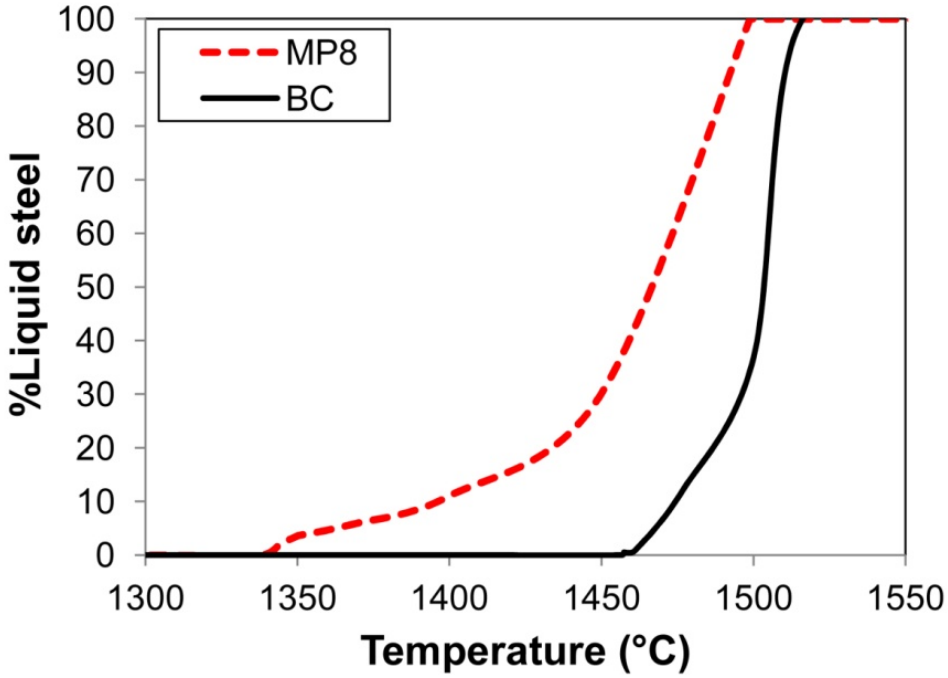

Figure 3. Effect of weld metal compositions on solidification curves: BC vs. MP8 weld metal compositions.

4. Discussion

4.1. Thermodynamics of Gas Phase Reactions

As displayed in Table 5, the yield percentage to the weld metal from the added metal powder is 91% Ni and 89% Cr. In our previous study on aluminium and nickel powders, the nickel yield was 85% [36]. These chromium and nickel yield numbers may be compared to the yield numbers achieved in the application of pre-alloyed powders in SAW [21]. The nickel yield values in SAW with pre-alloyed powders ranged from 59% to 78%, and chromium yield values varied from 58% to 76% when the "direct feeding" powder feed mode was applied [21]. This "direct feeding" mode is described as magnetically attaching the pre-alloyed powder to the weld wire as a surface coating, thus carrying the pre-alloyed powder with the weld wire into the arc cavity. Comparative welding tests were made for the two feeding modes using a pre-alloyed powder of the same composition, fed at the same feed rate, and using a single 2.5 mm diameter arcing weld wire at the same input weld parameters of 650 A, 32.2 V, and a 21 cm/min travel speed. The two feeding modes were "direct feeding" as described above vs. "forward feeding" in terms of feeding the powder onto the substrate steel plate, in advance of the welding head. The alloying element yields of Ni, Cr, and Mo to the weld metal were similar: in "forward feeding" mode, at 57% Ni yield, 56% Cr yield, and 55% Mo yield, vs. in "direct feeding" mode, at 59% Ni yield, 58% Cr yield, and 58% Mo yield [21]. In the following discussion, a thermodynamic analysis is applied to investigate the chemical interaction between nickel, chromium, and

aluminium. The effects of these chemical interations on the nickel and chromium yields to the weld metal are also investigated.

A variety of interdependent reactions take place in the arc cavity and may contribute to Ni, Cr, and Al loss in SAW. For example, some of the Ni, Cr, and Al may vaporise and also react with F_2(g) and/or CaF_2(g) to form NiF_2(g), CrF_2(g), CrF_3(g), AlF_3(g), AlF_2(g), and AlF(g). The Ni, Cr, and Al metal vapour may be oxidised to NiO, CrO, Cr_2O_3, and Al_2O_3. The following section shows how simple thermodynamic calculations were used to further investigate the relative likelihood of the possible reactions of Ni, Cr, and Al metal-fluoride formation, relative to similar reactions of the other main elements contained in the flux, metal powders, and steel. Reactions of the type in Equations (10) and (11) were considered and the Gibbs free energy graphs for these reactions are displayed in Figures 4 and 5. FactSage 7.3 thermochemical software was used to calculate the values in Figures 4 and 5 [30]. The temperature interval used in Figures 4 and 5, namely 1600 °C to 2500 °C, illustrates the temperature band of the main reactions in SAW as identified in previous works. It has been shown that the temperature of 2000 °C is the effective slag-metal equilibrium reaction temperature and the temperature of 2500 °C was reported as the maximum temperature at the interface between the arc plasma and the weld pool [2–4].

$$[Ni] + [F_2] = [NiF_2] \quad (10)$$

$$(NiO) + [CaF_2] = [NiF_2] + < CaO > \quad (11)$$

( ): liquid; []: gas; < >: solid.

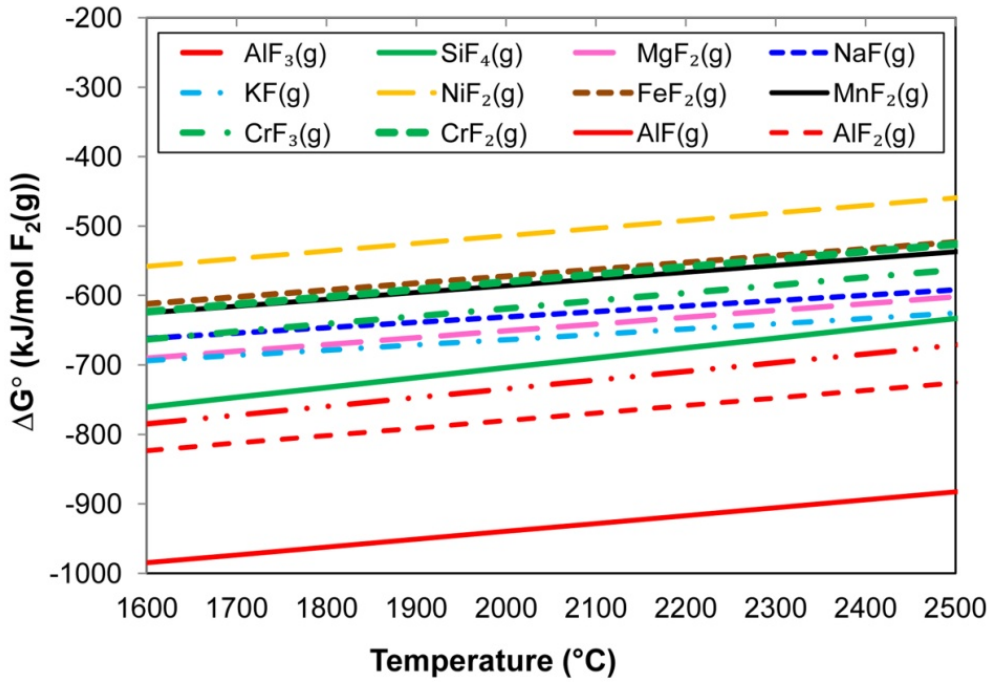

Figure 4. Standard Gibbs free energy values of reactions similar to Equation (10).

The following input values were applied in the calculation of the lines of reactions that are similar to Equation (10) in Figure 4: 1 atm for each gas, namely metal vapour, F_2(g), and the product metal fluoride gas. The calculation inputs for the lines for reactions that are similar to Equation (11), as displayed in Figure 5, were 1 atm CaF_2(g), unit activity for the molten metal oxides, 0.10 atm for the metal fluoride gas formed, and 0.01 activity for the CaO. The relative positions of the lines in Figure 4 show that formation of NiF_2(g) is least likely among the metal vapour reactions with F_2(g) and that aluminium-fluorides AlF_3(g), AlF_2(g), and AlF(g) are most probably formed. The formation of CrF_2(g) is less likely than

the formation of $CrF_3(g)$, with the $CrF_2(g)$ formation line in Figure 4 having very similar values as $FeF_2(g)$ and $MnF_2(g)$.

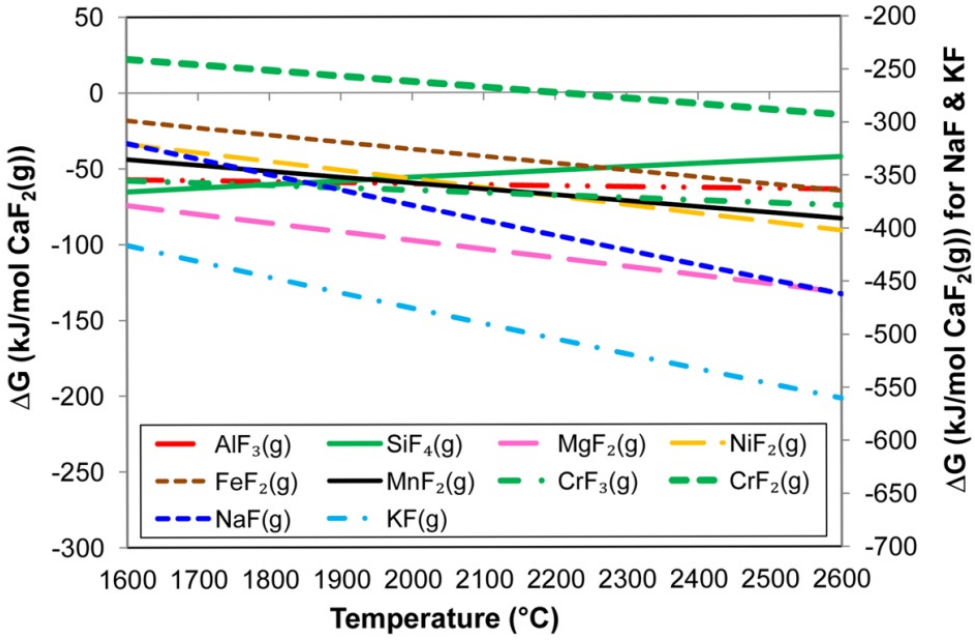

Figure 5. Gibbs free energy values of reactions similar to Equation (11).

Comparison of the Gibbs free energy values in Figure 4 to the values in Figure 5 indicates that all of the reactions of the type in Equation (10), as shown in Figure 4, are more likely to occur than reactions of the type in Equation (11), as shown in Figure 5. Therefore, the reaction of NiO with $CaF_2(g)$ is less probable than the reaction of Ni(g) with $F_2(g)$ to form $NiF_2(g)$. Similarly, a reaction of CrO or Cr_2O_3 with $CaF_2(g)$ is less probable than a reaction of Cr(g) with $F_2(g)$ to form $CrF_2(g)$ and $CrF_3(g)$, respectively. Because $AlF_3(g)$ formation is thermodynamically favoured relative to the considered metal fluorides in Figure 4, the implication is that Al vapour can react with the less thermodynamically stable metal fluorides to form $AlF_3(g)$ and metal vapour via reactions similar to the reaction displayed in Equation (12). The same argument holds for reactions of Al(g) and $CrF_3(g)$ and/or $CrF_2(g)$ to form Cr(g) in reactions similar to Equation (12).

$$2[Al] + 3[NiF_2] = 2[AlF_3] + 3[Ni] \quad (12)$$

The ease of aluminium vaporisation is shown in Figure 6. The vapour pressures of Al, Cr, and Ni, the main metal powder elements added into the SAW process, are compared to the vapour pressure of Fe, the main element in the carbon steel base plate and weld wire. The vapour pressure curves in Figure 6 were calculated in FactSage 7.3 thermochemical software using the ELEM database in the Reaction module [30]. Figure 6 confirms that aluminium is easily vaporised at the high temperatures that prevail in the arc cavity, which are 2000 °C to 2500 °C [2–4]. It can be seen that chromium is more easily vaporised than iron and nickel and therefore one may expect more primary vapour losses from metallic chromium than metallic nickel. Even though the potential of metal vaporisation is confirmed from the values in Figure 6, metal vapour may condense upon cooling of the gas, slag, and weld pool as the arc travels forwards along the weld path. Therefore, the values in Figure 6 are only indicative as a first order indication of pure metal vaporisation. Because a multitude of reactions may occur at the high temperatures that prevail in the arc cavity (beyond the simple reactions of type (10) to (12) and metal vaporisation), the following thermochemical simulation calculations were made.

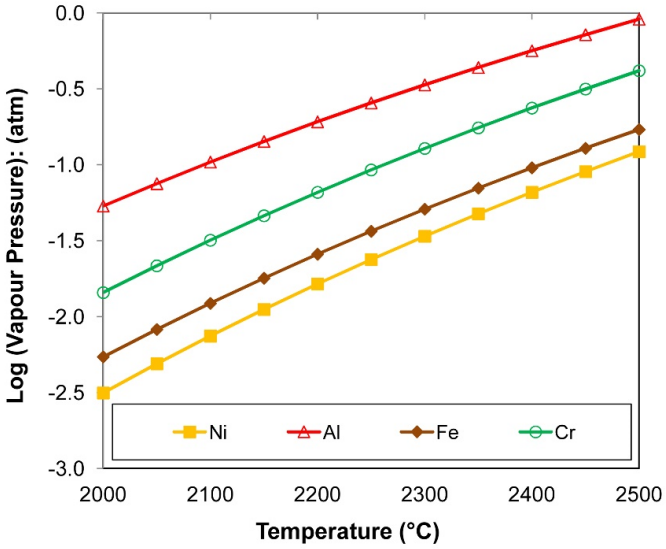

Figure 6. Pure metal elements of Al, Cr, Ni, and Fe vapour pressure.

The Equilib module in FactSage 7.3 thermochemical software was used to calculate the gas-slag-metal powder equilibrium between the molten flux (slag) and the alloy powders. The FToxid, FSstel, and FactPS databases were selected, as well as the inclusion of plasma species [30]. The flux input composition is shown in Table 2 and the flux mass input is equal to the slag mass measured for the post-weld slag. The nickel and chromium input masses of 7 g each were specified as feed into the weld run. The aluminium input mass in the calculation was varied between zero and the maximum of 6.3 g aluminium since the mass balance calculations showed that 0.72 g of the input 7 g of aluminium was consumed in reactions (5) and (6) (see Table 6). In addition, one may argue that the quantity of aluminium added into the weld metal did not participate in gas-based reactions. Therefore, one scenario was calculated to simulate this case at 3.10 g aluminium input. The calculated gas compositions and quantities are summarised in Table 7.

Table 7. Gas composition (volume %) output from gas-slag-metal powder equilibrium at 2500 °C calculated in FactSage 7.3 thermochemical software (Equilib module) [30].

Gram Al	%MgF_2	%MgF	%Mg	%AlF_3	%AlF_2	%AlF	%CaF_2	%NaF	%Na	%Mn	%MnF_2	%Ni	%Cr	%SiO
zero	13	8	10	2	4	6	12	5	5	7	1	7	7	8
3.10	4	7	19	1	4	16	5	2	4	7	<0.5	6	11	12
6.30	1	4	24	<0.5	2	22	2	1	4	6	<0.5	5	12	15

From the calculated gas speciation results displayed in Table 7, it appears that CaF_2(g) and MgF_2(g) are replaced by Mg(g), AlF(g), SiO(g), and Cr(g) due to the chemical interactions with the aluminium added into the arc cavity. The gas analysis calculation results in Table 7 indicate that increased aluminium added into the arc cavity can maintain more nickel and chromium in the metallic state, rather than in the form of oxides or fluorides. It appears that this effect is due to the lowered gas phase partial oxygen pressure resulting from aluminium metal additions, as summarised in the last column in Table 8. The result is that nickel and chromium metal vaporisation is favoured instead of NiF_2(g), CrF_2(g), and CrF_3(g) formation. The calculations show that gas formation increased with increased aluminium additions due to the aluminium-fluoride reactions. Because of the increased gas volumes, the nickel and chromium mass balance numbers shown in Table 8 prove that more nickel and chromium are vaporised at higher aluminium additions, even though the %Ni and %Cr in the gas changed to a smaller extent with increased aluminium, as displayed in

Table 7. From the calculated values shown in Table 8, it appears that a partial substitution of chromium for aluminium is possible, with maximum grams of aluminium reacting to the gas phase, chromium loss to the gas increasing from 26% to 40%, and aluminium loss to the gas phase decreasing from 57% to 50%. It is expected that only part of the feed aluminium powder reacts to form gas species in the arc cavity because according to the mass balance calculations, a significant portion of aluminium (67%, shown in Table 5) is directly alloyed into the weld metal. This aluminium proportion may have directly alloyed into the weld pool without first forming gas phase species.

Table 8. Expected metal loss to gas according to gas-slag-metal powder equilibrium at 2500 °C calculated in FactSage 7.3 thermochemical software (Equilib module) [30].

Gram Al	Mass %Ni to Gas	Mass% Cr to Gas	Mass% Al to Gas	Po_2 (atm)
zero	11	12	0.0	1.3×10^{-6}
3.10	15	26	57	2.4×10^{-7}
6.30	19	40	50	7.1×10^{-8}

4.2. Reaction Flow Diagram with Gas Reactions

The following discussion incorporates the findings from the above thermodynamic analysis on gas-based reactions into our SAW reaction flow diagram (Figure 7) for the application of nickel, chromium, and aluminium powders in an unconstrained format. Reaction steps A to E are as presented from previous works [4,12,16,17,22,29]. Reaction steps A to E represent oxygen transfer from the molten flux (slag) to the weld pool. Reaction A corresponds to the same type of reaction as in Equation (11), the reaction of Al_2O_3 with $CaF_2(g)$ to form $AlF_3(g)$ and CaO. This type of reaction is typically written in texts on fluoride-based welding fluxes, although the lowest Gibbs free energy values for Al-fluoride formation is as displayed in Figure 4 for the reaction of Al(g) with $F_2(g)$ via the reaction of the same type as that displayed in Equation (10).

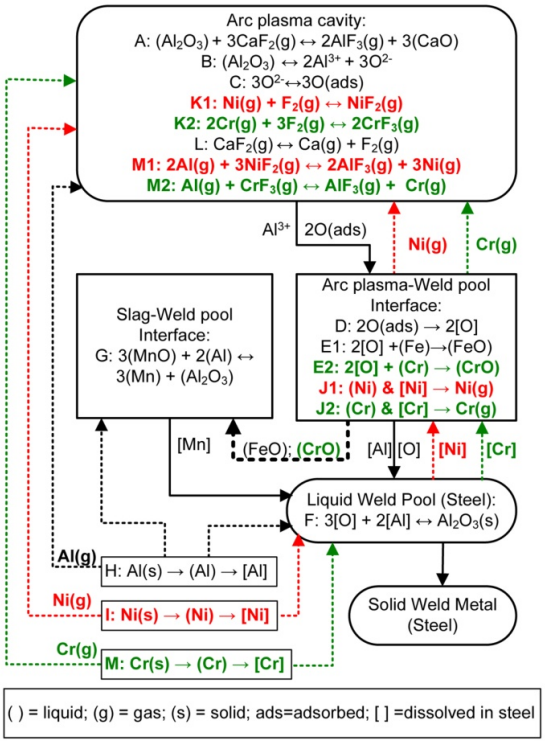

Figure 7. SAW reaction flow diagram with Al, Ni, and Cr powder additions [31].

Previous studies on SAW showed that an excessive quantity of oxygen is initially added to the molten weld wire droplets from the arc cavity gas phase, up to 2000–3000 ppm O [16,17]. Here, the word "excessive" means that the ppm O in the weld pool exceeds the solubility limit of oxygen in liquid steel at the temperatures that prevail in the weld pool as it cools down once the welding head has moved onward along the weld run. This is of importance because once the welding head has moved forward, there is no more arc energy input into the trailing weld pool, and it subsequently cools to lower temperatures from the high arc plasma temperatures that prevailed underneath the arc, typically 2000 °C–2500 °C [2–4]. This initial excessive oxygen quantity in the metal droplets is sourced from the decomposition of less stable oxides at the high temperatures that prevail in the arc plasma [16]. Based on the arc plasma stability hierarchy of oxides, MnO, SiO_2, MgO, and Al_2O_3 contained in the flux, as presented in Table 2, may all dissociate in the arc plasma to release oxygen in the arc cavity to adsorb onto the molten weld wire droplets, referring to reactions A to C shown in Figure 7 [18].

Previous works on SAW proved that the excessive quantity of oxygen transferred from the arc cavity to the weld pool reacts with the molten steel at the arc plasma–weld pool interface to form FeO, according to reaction E. This FeO is incorporated into the slag as proven by the correlation of increased FeO in the molten flux with increased weld metal total ppm O [22,29]. The oxygen potential that prevails at the molten flux–weld pool interface, as represented by the quantity of FeO in the slag, is reduced in this work by adding aluminium powder. Similar to reaction G for the reduction in the MnO content from the molten flux, FeO may also be reduced by aluminium; see reaction (7) in the text. These aluminium based reduction reactions, the reactions as displayed in Equations (5)–(8) in the text, are exothermic and therefore release chemical energy in the form of heat into the weld pool. This extra added heat can be used to melt and dissolve metal powder into the weld pool.

The reduced oxygen potential at the molten flux–weld pool interface prevents the oxidation of chromium powder to CrO and Cr_2O_3 and also prevents the oxidation of Ni to NiO to prevent chromium and nickel loss to the slag. Since Cr has a high affinity for oxygen, the formation of CrO may occur at the arc plasma–weld pool interface (reaction E2). However, it is expected that this CrO would be reduced by aluminium according to the reaction similar to reaction G in Figure 7, the same as reaction (8) shown in Section 3.3 [32,34,35]. Therefore, due to the chemical action of aluminium, the nickel and chromium powders are melted and dissolved into the weld pool; see reactions I and M. Since there is an excess of Al added, some of the Al also directly dissolves into the weld pool; see reaction H.

Based on the Gibbs free energy values displayed in Figures 4 and 5, it appears that chromium and nickel loss in SAW, with the addition of metal powder alloying, occurs due to chromium and nickel vaporisation and/or subsequent reaction of chromium and nickel vapour with Fluorine gas to form CrF_2(g), CrF_3(g), and NiF_2(g). This reaction sequence is marked in Figure 7 in red text as reactions J1 and K1 for nickel reactions and in green text as reactions J2 and K2 for chromium reactions, in combination with reaction L for F_2(g) release from CaF_2(g) dissociation. The formation of F_2(g) in the arc cavity from the dissociation of CaF_2(g) in the arc plasma appears possible since Ca and F were analysed in the arc cavity gas phase when a CaF_2-based flux was used in SAW test runs [1,39].

Aluminium vapour may react with the chromium and nickel fluorides, CrF_2(g), CrF_3(g), and NiF_2(g), to transform these fluorides to nickel and chromium vapour via reactions similar to Equation (12), presented by reactions M1 and M2 shown in Figure 7. Chromium and nickel can be vaporised from the weld pool, at the arc plasma–weld pool interface, and from the unconstrained metal powders before dissolution of the metal powders into the weld pool. This conclusion is confirmed by the gas speciation calculation results from gas-slag-metal powder calculations as summarised in Table 7.

The added aluminium powder plays a role in gas phase reactions to shift chromium and nickel powders to the vapour phase instead of the oxidation of chromium and nickel powders to CrO, Cr_2O_3, and NiO, as discussed for the thermodynamic analysis in the

above section. Despite this important role of aluminium in gas phase reactions, the final deciding factor on the oxidation state of chromium and nickel is the partial oxygen pressure at the molten flux–weld pool interface. The reason for this conclusion is that the final weld pool influencing reactions occur at the molten flux–weld pool interface as the weld pool cools down from the high arc plasma temperatures to the weld pool solidus temperature.

The results presented here are in agreement with our previous similar works on the SAW process in which different metal powder combinations with aluminium were applied [31–37]. The results show that the oxygen potential at the molten flux–weld pool interface is lowered by aluminium powder addition. The importance of this effect of aluminium plays a critical role in the transfer of chromium and nickel into the weld pool, without interfering with oxygen transfer from the plasma arc to the weld pool. The latter point is important in SAW because some level of total ppm O is required in the weld metal to form oxide inclusions for AF nucleation [6,14,15]. This is in contrast with the typically low total oxygen of 30 ppm O achieved in aluminium-killed Cr-alloyed steel [24]. The thermodynamic analysis presented here shows that the likely chemical reaction of chromium and nickel loss is due to a reaction of chromium and nickel vapour with F_2(g) to form CrF_2(g), CrF_3(g), and NiF_2(g) in the arc cavity, and not due to the formation of CrO, Cr_2O_3, and NiO as intermediate compounds. Furthermore, CrF_2(g), CrF_3(g), and NiF_2(g) in the arc cavity may be easily transformed to chromium and nickel vapour via reactions of the type in Equation (12). The main chemical interaction between chromium and nickel with aluminium indirectly occurs via lowering of the oxygen potential at the molten flux–weld pool interface, which in turn ensures that chromium and nickel are maintained as metallic species. The lowered oxygen potential prevents chromium and nickel oxidation from the weld pool to oxides, such as CrO, Cr_2O_3, and NiO, preventing chromium and nickel loss to the slag via oxidation.

5. Conclusions

1. The application of unconstrained Al, Cr, and Ni metal powders in SAW result in improved chromium and nickel yields to the weld metal. Chromium and nickel yield values achieved here with aluminium additions are higher than the literature's reported values achieved with pre-alloyed iron-chromium-nickel powders.
2. Carbon steel weld metal was alloyed with unconstrained metal powders to 6.2% Ni, 6.0% Cr, and 4.5% Al to achieve a 91% Ni yield, 89% Cr yield, and 67% Al yield to the weld metal.
3. It was confirmed that the aluminium powder added into the SAW process was performed effectively to sufficiently control the oxygen potential at the molten flux–weld pool interface, without interfering with oxygen transfer from the arc plasma to the weld pool. The weld metal total oxygen content was controlled to 162 ppm O in MP8 weld metal vs. 499 ppm O in the weld metal formed in the absence of metal powder additions.
4. At the high temperatures of the arc cavity, Cr and Ni in the form of metal vapour are thermodynamically favoured over NiF_2(g), CrF_2(g), and CrF_3(g) formation because Al-fluorides are thermodynamically more stable. In addition, the low partial oxygen pressure (maintained by Al additions) prevents the oxidation of Cr and Ni.
5. The application of unconstrained metal powders in SAW can improve overall process productivity because unconstrained metal powders can be directly applied in the SAW process, thus removing the need for the manufacturing of alloyed wire and alloyed powder as expensive time consuming steps.

Author Contributions: F.D.B. conceptualised the work as the inventor; F.D.B. and T.C. executed the experiments, interpreted the data, and prepared the manuscript. All authors have read and agreed to the published version of the manuscript.

Funding: This research was funded in part by the National Research Foundation of South Africa, grant number BRIC171211293679.

Data Availability Statement: The datasets presented in this study are available upon reasonable request to the corresponding author, indicated on the first page.

Conflicts of Interest: The authors declare no conflict of interest. The funders had no role in the design of the study; in the collection, analyses, or interpretation of data; in the writing of the manuscript, or in the decision to publish the results.

References

1. Sengupta, V.; Havrylov, D.; Mendex, P.F. Physical phenomena in the weld zone of submerged arc welding—A Review. *Weld. J.* **2019**, *98*, 283–313.
2. Chai, C.S.; Eagar, T.W. Slag-metal equilibrium during submerged arc welding. *Metall. Trans. B* **1981**, *12*, 539–547. [CrossRef]
3. Mitra, U.; Eagar, T.W. Slag-metal reactions during welding: Part I. Evaluation and reassessment of existing theories. *Metall. Trans. B* **1991**, *22*, 65–71. [CrossRef]
4. Mitra, U.; Eagar, T.W. Slag-metal reactions during welding: Part II. Theory. *Metall. Trans. B* **1991**, *22*, 73–81. [CrossRef]
5. Mitra, U.; Eagar, T.W. Slag-metal reactions during welding: Part III. Verification of the theory. *Metall. Trans. B* **1991**, *22*, 83–100. [CrossRef]
6. Kluken, A.O.; Grong, Ø. Mechanisms of inclusion formation in Al-Ti-Si-Mn deoxidized steel weld metals. *Metall. Trans. B* **1989**, *20*, 1335–1349. [CrossRef]
7. Chai, C.S.; Eagar, T.W. The effect of SAW parameters on weld metal chemistry. *Weld. J.* **1980**, *59*, 93–98.
8. Singh, B.; Khan, Z.A.; Siddiquee, A.N. Effect of flux composition on element transfer during Submerged Arc Welding (SAW): A literature review. *Int. J. Curr. Res.* **2013**, *5*, 4181–4186.
9. Palm, J.H. How fluxes determine the metallurgical properties of Submerged Arc Welds. *Weld. J.* **1972**, *51*, 358–360.
10. Paniagua-Mercado, A.M.; Lopez-Hirata, V.M.; Saucedo Munoz, M.L. Influence of the chemical composition of flux on the microstructure and tensile properties of submerged-arc welds. *J. Mater. Process. Technol.* **2005**, *169*, 346–351. [CrossRef]
11. Bang, K.; Park, C.; Jung, H.; Lee, J. Effects of flux composition on the element transfer and mechanical properties of weld metal in submerged arc welding. *J. Met. Mater. Int.* **2009**, *15*, 471–477. [CrossRef]
12. Eagar, T.W. Sources of weld metal oxygen contamination during submerged arc welding. *Weld. J.* **1978**, *57*, 76–80.
13. Tuliani, S.S.; Boniszewski, T.; Eaton, N.F. Notch toughness of commercial submerged arc weld metal. *Weld. Met. Fabr.* **1969**, *37*, 327–339.
14. Dallam, C.B.; Liu, S.; Olson, D.L. Flux composition dependence of microstructure and toughness of submerged arc HSLA weldments. *Weld. J.* **1985**, *64*, 140–152.
15. Chovet, A.; Galand, E.; Leduey, B. Effect of various factors on toughness in P92 SAW weld metal. *Weld. World* **2008**, *52*, 18–26. [CrossRef]
16. Polar, A.; Indacochea, J.E.; Blander, M. Electrochemically generated oxygen contamination in submerged arc welding. *Weld. J.* **1990**, *69*, 68–74.
17. Lau, T.; Weatherly, G.C.; Mc Lean, A. The sources of oxygen and nitrogen contamination in submerged arc welding using CaO-Al_2O_3 based fluxes. *Weld. J.* **1985**, *64*, 343–347.
18. Chai, C.S.; Eagar, T.W. Slag metal reactions in binary CaF_2-metal oxide welding fluxes. *Weld. J.* **1982**, *61*, 229–232.
19. ESAB: Technical Handbook Submerged Arc Welding. 2021. Available online: https://assets.esab.com/asset-blank/assetfile/12295.pdf (accessed on 13 June 2021).
20. O'Brien, A. *Welding Handbook, Part 1*, 9th ed.; American Welding Society (AWS): Miami, FL, USA, 2004.
21. Hallén, H.; Johansson, K.-E. Use of a Metal Powder for Surface Coating by Submerged Arc Welding. U.S. Patent 6331688 B1, 18 December 2001.
22. Mitra, U.; Eagar, T.W. Slag metal reactions during submerged arc welding of alloy steels. *Metall. Trans. B* **1984**, *15*, 217–227. [CrossRef]
23. Burck, P.A.; Indacochea, J.E.; Olson, D.L. Effects of welding flux additions on 4340 steel weld metal composition. *Weld. J.* **1990**, *69*, 115–122.
24. Lee, S.-B.; Choi, J.-H.; Jung, S.-M.; Lee, H.-G.; Rhee, P.C.-H. Aluminium deoxidation equilibrium on liquid Fe-16 Pct Cr alloy. *Metall. Trans. B* **2005**, *36*, 414–416. [CrossRef]
25. Pramanik, S.; Suwas, S. Low-density steels: The effect of Al addition on microstructure and properties. *JOM* **2014**, *66*, 1868–1876. [CrossRef]
26. Moon, J.; Ha, H.-Y.; Kim, K.-W.; Park, S.-J.; Lee, T.-H.; Kim, S.-D.; Jang, J.H.; Jo, H.-H.; Hong, H.-U.; Lee, B.H.; et al. A new class of lightweight, stainless steels with ultra-high strength and large ductility. *Sci. Rep.* **2020**, *10*, 12140. [CrossRef] [PubMed]
27. Raabe, D.; Tasan, C.C.; Springer, H.; Bausch, M. From high-entropy alloys to high-entropy steels. *Steel Res. Int.* **2015**, *86*, 1127–1138. [CrossRef]
28. Coetsee, T. Phase chemistry of Submerged Arc Welding (SAW) fluoride based slags. *Mater. Res. Technol.* **2020**, *9*, 9766–9776. [CrossRef]
29. Coetsee, T.; Mostert, R.J.; Pistorius, P.G.H.; Pistorius, P.C. The effect of flux chemistry on element transfer in Submerged Arc Welding: Application of thermochemical modelling. *Mater. Res. Technol.* **2021**, *11*, 2021–2036. [CrossRef]

30. Bale, C.W.; Bélisle, E.; Chartrand, P.; Decterov, S.; Eriksson, G.; Gheribi, A.E.; Hack, K.; Jung, I.-H.; Kang, Y.-B.; Melançon, J.; et al. Reprint of: FactSage thermochemical software and databases, 2010–2016. *Calphad* **2016**, *55*, 1–19. [CrossRef]
31. Coetsee, T.; De Bruin, F.J. Improved titanium transfer in Submerged Arc Welding of carbon steel through aluminium addition. *Miner. Process. Extr. Metall. Rev.* **2021**, *43*, 771–774. [CrossRef]
32. Coetsee, T.; De Bruin, F.J. Reactions at the molten flux-weld pool interface in submerged arc welding. *High Temp. Mater. Processes.* **2021**, *40*, 421–427. [CrossRef]
33. Coetsee, T.; De Bruin, F. Application of Copper as Stabiliser in Aluminium Assisted Transfer of Titanium in Submerged Arc Welding of Carbon Steel. *Processes* **2021**, *9*, 1763. [CrossRef]
34. Coetsee, T.; De Bruin, F. Chemical Interaction of Cr-Al-Cu Metal Powders in Aluminum-Assisted Transfer of Chromium in Submerged Arc Welding of Carbon Steel. *Processes* **2022**, *10*, 296. [CrossRef]
35. Coetsee, T.; De Bruin, F. Aluminium-Assisted Alloying of Carbon Steel in Submerged Arc Welding: Application of Al-Cr-Ti-Cu Unconstrained Metal Powders. *Processes* **2022**, *10*, 452. [CrossRef]
36. Coetsee, T.; De Bruin, F. Aluminium Assisted Nickel Alloying in Submerged Arc Welding of Carbon Steel: Application of Unconstrained Metal Powders. *Appl. Sci.* **2022**, *12*, 5392. [CrossRef]
37. Coetsee, T.; De Bruin, F. Application of Unconstrained Cobalt and Aluminium Metal Powders in the Alloying of Carbon Steel in Submerged Arc Welding: Thermodynamic Analysis of Gas Reactions. *Appl. Sci.* **2022**, *12*, 8472. [CrossRef]
38. Coetsee, T.; De Bruin, F. In Situ Modification of CaF_2-SiO_2-Al_2O_3-MgO Flux Applied in the Aluminium-Assisted Transfer of Titanium in the Submerged Arc Welding of Carbon Steel: Process Mineralogy and Thermochemical Analysis. *Minerals* **2022**, *12*, 604. [CrossRef]
39. Gött, G.; Gericke, A.; Henkel, K.-M.; Uhrlandt, D. Optical and spectroscopic study of a submerged arc welding cavern. *Weld. J.* **2016**, *95*, 491–499.